First AC loss test and analysis of a Bi2212 cable-in-conduit conductor for fusion application

Jinggang Qin[1] , **Yi Shi**[1,5], **Yu Wu**[1], **Jiangang Li**[1], **Qiuliang Wang**[2], **Yuxiang He**[1], **Chao Dai**[1], **Fang Liu**[1], **Huajun Liu**[1,5], **Zhehua Mao**[1], **Arend Nijhuis**[3], **Chao Zhou**[3] and **Arnaud Devred**[4]

[1] Institute of Plasma Physic, Chinese Academy of Sciences, Hefei, Anhui, 230031, People's Republic of China
[2] Institute of Electrical Engineering, Chinese Academy of Sciences, Beijing, 100190, People's Republic of China
[3] University of Twente, Energy, Materials and Systems, Faculty of Science and Technology, Enschede, 7500AE, Netherlands
[4] CERN, TE Department, Geneva 23 1211, Switzerland

E-mail: shiyi@ipp.ac.cn and liuhj@ipp.ac.cn

CrossMark

Abstract

The main goal of the Chinese fusion engineering test reactor (CFETR) is to build a fusion engineering tokamak reactor with a fusion power of 50–200 MW, and plan to test the breeding tritium during the fusion reaction. This may require a maximum magnetic field of the central solenoid and toroidal field coils up to 15 T. New magnet technologies should be developed for the next generation of fusion reactors with higher requirements. $Bi_2Sr_2CaCu_2O_x$ (Bi2212) is considered as a potential and promising superconductor for the magnets in the CFETR. R&D activities are ongoing at the Institute of Plasma Physics, Chinese Academy of Sciences for demonstration of the feasibility of a CICC based on Bi2212 round wire. One sub-size conductor cabled with 42 wires was designed, manufactured and tested with limited strand indentation during cabling and good transport performance. In this paper, the first test results and analysis on the AC loss of Bi2212 round wires and cabled conductor samples are presented. Furthermore, the impact of mechanical load on the AC loss of the sub-size conductor is investigated to represent the operation conditions with electromagnetic loads. The first tests provide an essential basis for the validation of Bi2212 CICC and its application in fusion magnets.

Keywords: Bi2212 CIC conductor, AC loss, CFETR

(Some figures may appear in colour only in the online journal)

1. Introduction

The Chinese fusion engineering test reactor (CFETR) is a new tokamak device in China with the goals of 50–200 MW fusion power and self-sufficiency [1, 2]. Its major radius of plasma is 5.7 m, and minor radius of plasma is 1.6 m. The central magnetic field is 5–7 T [3]. The magnet system consists of sixteen toroidal field coils (TF), a central solenoid (CS), which consists of six coils and six poloidal field coils (PF) [3]. As one of the core components of the CFETR, superconducting magnet technology is a big challenge, especially for the CS and TF coils which need to fulfill the requirement of a maximum magnetic field of around 15 T, which is significantly higher than that of present fusion magnets like ITER. New superconductors, especially high temperature superconductors (HTS) and related magnet technology, are being considered for development and application for next generation fusion magnets.

[5] Authors to whom any correspondence should be addressed.

Fusion based magnetic fields above 16 T are beyond the realistic capability of present Nb-based superconducting materials. Bi2212 is a promising material for the development of superconducting magnets in the 20 T range [4, 5] due to the high upper critical magnetic field. However, apart from the superconductor materials, the materials for the coil structures need to be further developed to withstand the enormous stresses in addition. Compared to Nb_3Sn for the same peak magnetic field in the range of 12–18 T, Bi2212 has a larger temperature margin during operation of the reactor magnet system. Moreover, Bi2212 is also the only cuprate superconductor that can be made into round wire (RW), which makes it possible to develop a CICC with Bi2212 round wire [6, 7]. At present, CICCs are mainly made of Nb_3Sn and NbTi strands, such as ITER conductors [8, 9]. In 2003, JAEA developed a Bi2212 cable with 729 wires, reaching a critical current, I_c, of 10 kA at 12 T and 20 K [10]. After that, a few more studies on Bi2212 cables were conducted [11–14]. However, difficulties in manufacturing a Bi2212 CICC are the high strain sensitivity of Bi2212 [15–17], unavoidable strand deformation during the cabling and the material selection for the jacket [14, 18] due to the aging of Bi2212 by oxygen during heat treatment.

As a first trial in the technology development of Bi2212 CICC, one sub-size CICC conductor with 42 Bi2212 round wires has been manufactured. The conductor performed well in terms of controlled strand indentation and deformation during cabling, which resulted in acceptable critical currents [19]. In this paper, the focus is on the test and investigation of the AC loss of the Bi2212 CICC. First, the AC loss of the Bi2212 round wires has been measured at several temperatures and with perpendicular and parallel applied magnetic fields with a vibrating sample magnetometer (VSM) from Physical Property Measurement System (PPMS). Then, the test and analysis of the AC loss of Bi2212 CIC conductor samples are presented, also at 4.2 K and for perpendicular and parallel applied magnetic fields. Furthermore, mechanical transverse load was applied on sub-size conductor samples to evaluate the influence on the AC loss, as a representation of the operation conditions under applied electromagnetic (EM) loads. As a result, the coupling and hysteresis loss parameters are provided to assess the Bi2212 CICC performance and its potential application for fusion magnets.

2. Bi2212 wire, cable and conductor

The Bi2212 RW was manufactured using the powder in tube method by the Northwest Institute for Non-ferrous Metal Research. The cross-sectional micrographs are shown in figure 1 for the wires before and after heat treatment and their parameters are listed in table 1. For the CICC design, performance degradation in terms of critical current is the main issue due to the high strain sensitivity and brittleness of Bi2212. The layout of the cable initially followed the ITER CS short twist pitch design [8], which improved the issue of performance degradation under EM loads. The parameters of Bi2212 cable for the first three stages with 42 wires are shown in table 2.
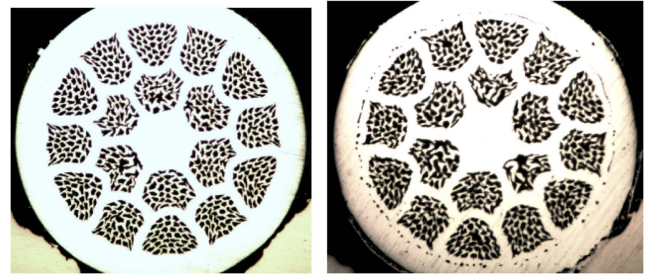

Figure 1. The cross-sectional micrographs of unreacted (left) and reacted (right) Bi2212 round wire.
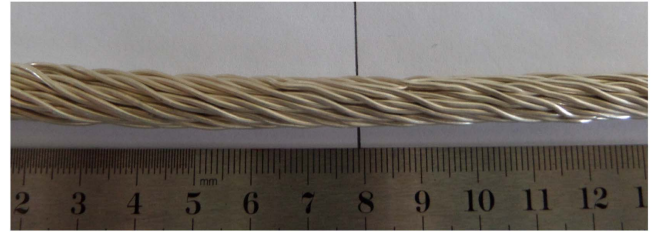

Figure 2. The final Bi2212 cable (the 3rd stage).

Table 1. Parameters of the tested Bi2212 wire.

Material	Ag-alloy sheathed Bi2212
Diameter	1.0 mm
Filament configuration	19×18
Ag/Mg:Ag:Bi2212	1.8:1:0.9
I_c at 0 T, 4.2 K	about 400 A
I_c at 12 T, 4.2 K	about 146 A

Table 2. Parameters of the sub-size cable.

Item	Parameter
Layout	$2 \times 3 \times (6 + 1)$
Twist pitch	
Stage 1	20 mm
Stage 2	50 mm
Stage 3	87 mm
Diameter (no compaction)	10 mm
Diameter (after compaction)	9.0 mm

The cable has a three-stage layout without a central spiral. The final cable was compacted by rollers with a special shape in order to control the deformation of the cable surface and with possible damage. The final cable is shown in figure 2.

The Bi2212 cable was inserted into a jacket with a circular cross-section. Because the Bi2212 is heat-treated in an oxygen environment, the Bi2212 wire cannot be in contact with common stainless steel (e.g. 316L or 316LN) during heat treatment since this will reduce the critical current. Consequently, an Ag tube was used to separate the cable and SS jacket as shown in figure 3. The conductor was heat treated at $T_{max} = 890\,°C$ for 30 min. Then the temperature was reduced
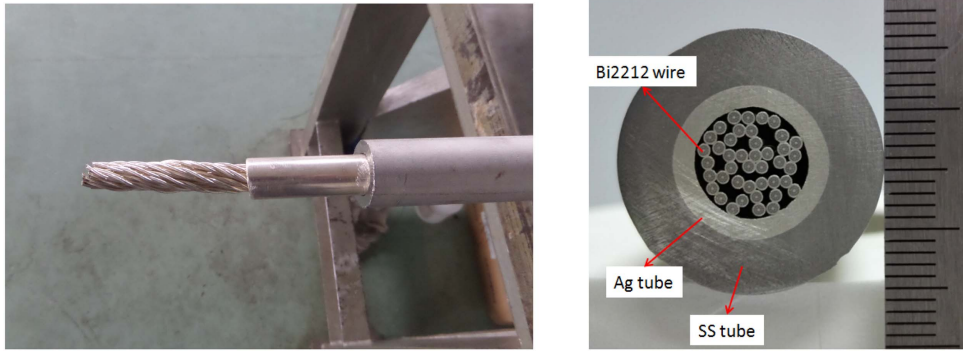
Figure 3. The Bi2212 conductor with SS jacket outside and Ag tube in between (left) and its transverse cross-section view (right).

to 830 °C with a rate of 5 °C h^{-1}, and then kept on a plateau at $T_{max} = 830$ °C for 48 h in a standard oxygen environment.

The first critical current (I_c) test was performed at liquid helium (4.2 K) and self-field due to limited testing conditions. The I_c of the sub-size Bi2212 CICC is found to be 13.1 kA with an *n*-value of 12, while according to the witness wire I_c at 4.2 K in conductor self-field amounts to 15.4 kA (the single wire *n*-value is 13). This means a 15% degradation of I_c for the conductor after cabling and compaction. This could be attributed to wire deformation during manufacture or even partly due to difficulties in heat treatment, which is more demanding than for a short wire length.

In order to obtain the AC loss of the conductor, similar wire and conductor samples were tested at the University of Twente.

3. AC loss of Bi2212 round wire

AC loss measurements of the Bi2212 round wire were performed at various temperatures (4.2, 20, 50 and 77 K) with parallel and perpendicular applied magnetic fields in a PPMS-VSM [20], with a suitable testing insert for Bi2212 wire following the required specifications [21]. The tested samples are straight Bi2212 round wire pieces with a length of ~5 mm. The time varying magnetic field has a triangular shape with amplitude up to 9 T applied perpendicular and parallel to the specimen axis, with different sweep rates ranging from 1 to 20 mT s^{-1} for analyses of the hysteresis and coupling loss.

The results of the AC loss measurements with magnetic field (B) from −1 to 9 T at temperatures (T) of 4.2, 20, 50, 77 K and ramp rate of 20 mT s^{-1} are shown in figures 4 and 5 for a sample length of ~4.9 mm, for magnetic field orientation in parallel and perpendicular direction, respectively. The measured magnetic moment at different temperatures and fields indirectly reflects the relation of I_c corresponding to T and B.

To investigate the coupling loss at different temperatures, AC loss measurements are conducted with magnetic field amplitude from −3 to 3 T and different ramp rates at 4.2, 20 and 50 K with the magnetic field in a perpendicular orientation (see figures 6 to 8). The same measurements were
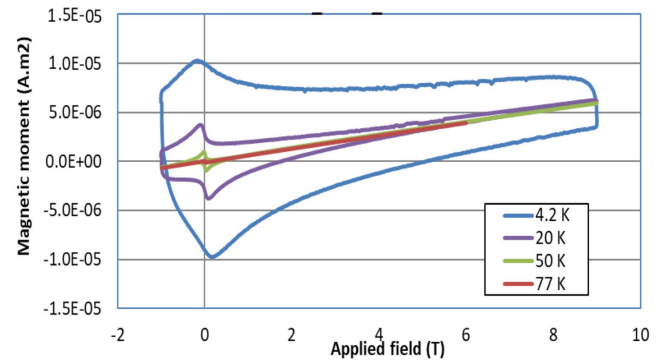

Figure 4. AC loss measurements with the magnetic field parallel with the sample's axis; the sample length is 4.89 mm, B = −1 to 9 T, T = 4.2, 20, 50, 77 K, ramp rate = 20 mT s^{-1}.
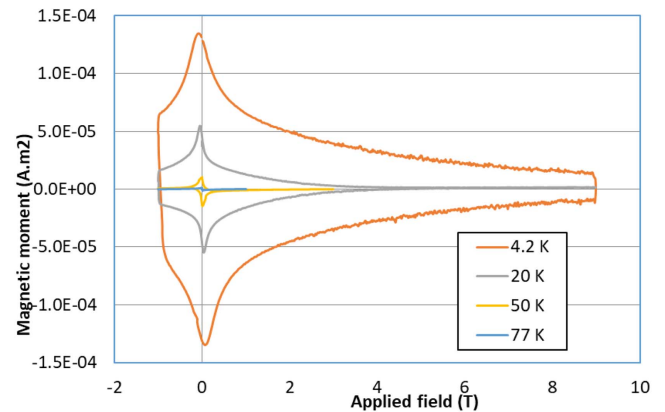

Figure 5. AC loss measurements with the magnetic field perpendicular to sample's axis; the sample length is 4.90 mm, B = −1 to 9 T, T = 4.2, 20, 50, 77 K, ramp rate = 20 mT s^{-1}.

performed with the field parallel to the sample axis. When no transport current is considered and only an external time varying magnetic field is applied to the sample, the hysteresis loss per cycle at low excitation (e.g. below than 100 mT s^{-1}) is independent of the ramp rate and the coupling loss can then be separated from the hysteresis loss by applying different frequencies [22, 23].

For a triangular field cycle with amplitude Ba, the coupling loss Q_c in terms of energy loss per unit volume and per
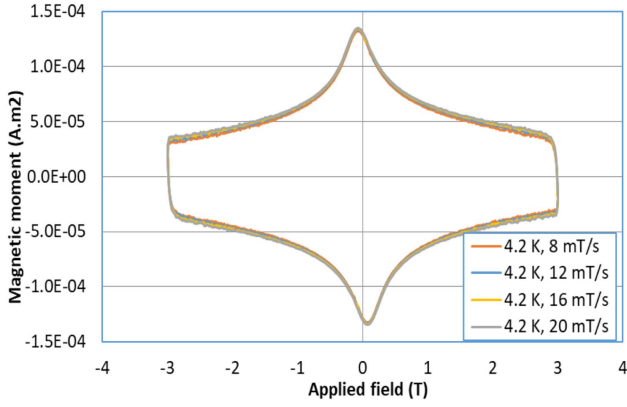
Figure 6. AC loss measurements with magnetic field perpendicular to the sample axis with a sample length of 4.901 mm, B = −3 to 3 T, T = 4.2 K, ramp rate = 8, 12, 16, 20 mT s^{-1}.
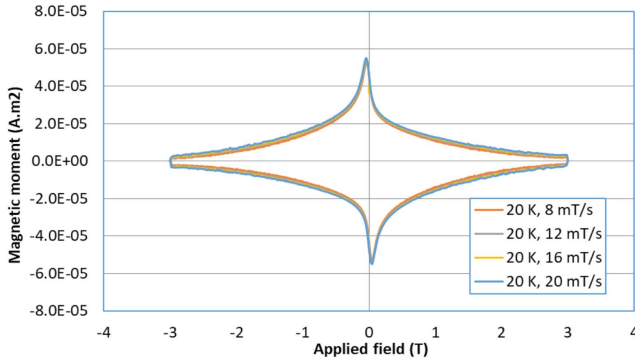

Figure 9. Coupling loss investigation with magnetic field perpendicular to the sample's axis at a sample length of 4.901 mm, T = 4.2, 20, 50 K, ±3 T.

Figure 7. AC loss measurements with magnetic field perpendicular to the sample axis with a sample length of 4.901 mm, B = −3 to 3 T, T = 20 K, ramp rate = 8, 12, 16, 20 mT s^{-1}.
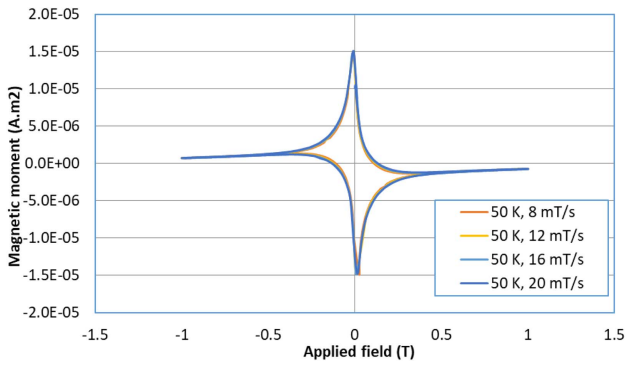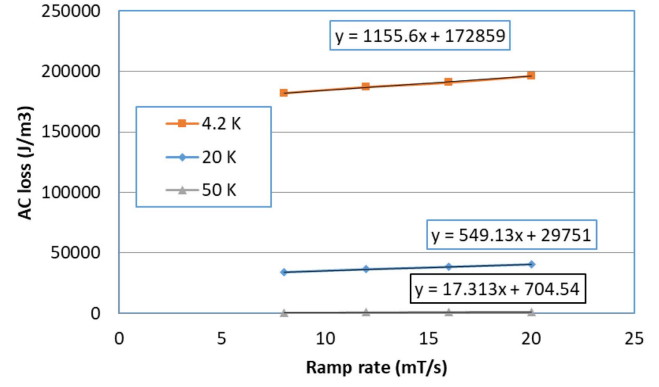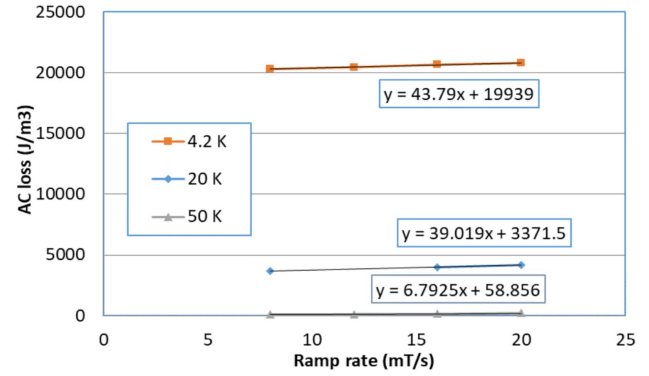

Figure 10. Coupling loss investigation with magnetic field parallel with the sample's axis at a sample length of 4.890 mm, T = 4.2, 20, 50 K, ±3 T.

Figure 8. AC loss measurements with magnetic field perpendicular to the sample axis with a sample length of 4.901 mm, B = −3 to 3 T, T = 50 K, ramp rate = 8, 12, 16, 20 mT s^{-1}.

applied field cycle can be written as:

$$Q_c = \frac{2n\tau}{\mu_0} \Delta B \frac{dB_a}{dt} \qquad (1)$$

where μ_0 is the permeability in vacuum (H m^{-1}); $n\tau$ is the effective coupling current loss time constant, which can be

written as [22] for a triangular field cycle of amplitude Ba:

$$n\tau = \frac{\alpha\mu_0}{2\Delta B} \qquad (2)$$

and α is the slope of the initial linear section of the total AC loss against the magnetic field ramp rate, the shape factor of the round conductors is represented by n and approaches 2.

The AC loss versus frequency is indicated in figures 9 and 10 for the tested Bi2212 wire sample with a length of ∼4.9 mm. The intersection with the loss axis represents the hysteresis loss Q_h while the initial slope of the line represents the coupling loss. According to the slopes in figures 9 and 10 as well as equation (2), the coupling loss time constant $n\tau$ with magnetic field perpendicular with sample axis are 121, 58 and 5.4 ms for 4.2, 20 and 50 K respectively. For parallel magnetic field direction the $n\tau$ amounts to 4.58, 4.09 and 0.71 ms for 4.2, 20 and 50 K, respectively. The $n\tau$ of Bi2212 wire at 4.2 K is around one order of magnitude higher than that of Nb$_3$Sn wire due to the much lower matrix (silver) resistivity in Bi2212 wire than that (bronze) for Nb$_3$Sn wire.
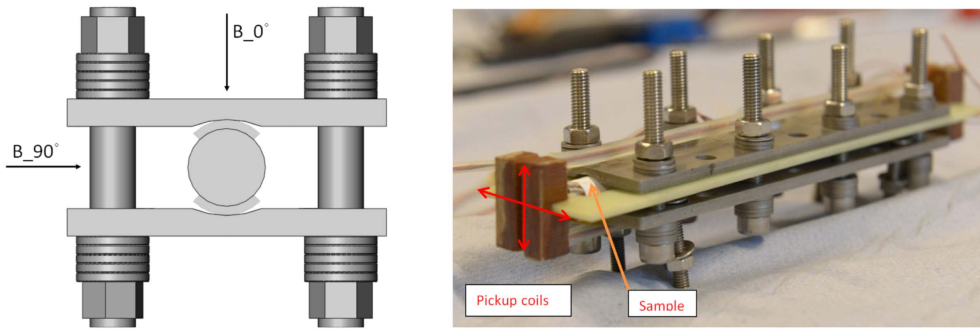
Figure 11. Schematic view and photo of the transverse load setup with the Bi2212 conductor sample.

4. AC loss of Bi2212 CIC conductor

Knowledge of the AC loss and influence of transverse load on the AC loss is inevitable to gain sufficient confidence in an economic design and stable operation of this conductor [24–29]. The AC loss has been measured in the standard magnetization magnet for transverse magnetic fields in a recently constructed setup at the University of Twente [30].

The jacket was removed before heat treatment in order to match the testing conditions. To check the conductor homogeneity along its length it was cut into three sections with equal length after the first measurement of the AC loss on the whole length (around 418 mm) and without load. The AC loss of each section was measured individually under the same conditions. The influence of the Lorentz force on the conductor was simulated by applying transverse load on one section of the conductor. The AC loss behavior under applied transverse load was measured for two magnetic field versus force orientations; transverse and parallel.

4.1. Experimental set-ups

The AC loss is measured by a gas flow calorimeter [30], which measures the power dissipation in the conductor by a calibrated gas flow of helium boil-off. The calorimeter is inserted in the bore of a superconducting dipole and the measurements are carried out at 4.2 K with a sinusoidal modulation field of 0.4 T amplitude with/without an offset field of 1 T. Besides the calorimetric measurement of the power dissipation, a magnetization loop is obtained by means of a compensated pickup coil wound around the conductor. To calibrate the magnetization data, the calorimetric data obtained with the same sample at higher frequencies giving power dissipation in the sample higher than 10 mW for sufficient accuracy were used.

A transverse load was applied to the sample by clamping the sample between two stainless steel plates with grooves. The transverse load simulates the influence of the Lorentz force. The two plates are pressed together using stainless steel bolts and nuts and a set of titanium rings. The specific choice of titanium rings follows from the difference in thermal contraction coefficient between stainless steel and titanium. When the setup is cooled down, the stainless steel contracts more than the titanium, which results in a larger stress on the sample. Prior to cool-down, the sample is pre-stressed at room
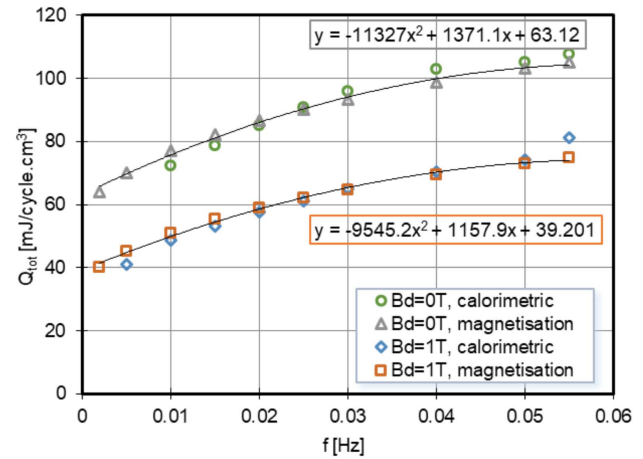

Figure 12. Total AC loss as a function of the applied magnetic field frequency for the whole conductor section before cutting it into three sections. The lines through the data are second order polynomial fits with the equations given in the plot.

temperature. The stress is measured by means of deformation of the top stainless steel plate by three calibrated strain gauges attached to the plate, and thus derivate the applied stress on the cable from the plates.
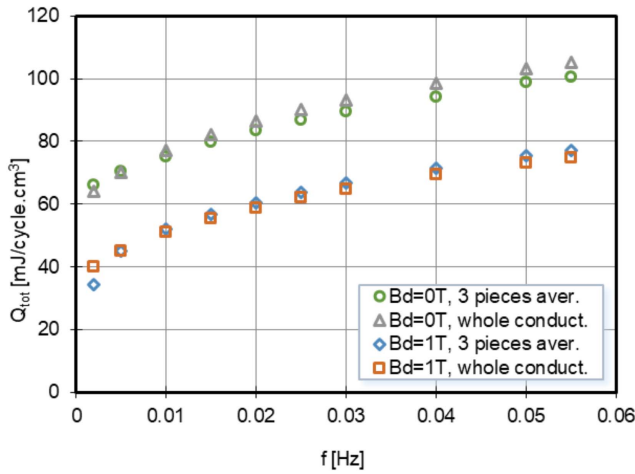
A Teflon tape was wound around the sample to avoid a local extreme in the applied stress due to a quasi line contact. The Teflon layer causes a smearing effect resulting into a more uniform applied stress. Two pickup coils, perpendicularly oriented to each other, were wound around the sample to measure the sample magnetization. Figure 11 shows the schematic view of the transverse load setup and a photo of the setup with the positions of the pickup coils marked.

4.2. AC loss measurement results

Figure 12 shows the total AC loss for the whole conductor sample before cutting into sections as a function of the applied magnetic field frequency. The measured loss is normalized per volume Bi2212 cable made by 42 strands and a conductor length of 418 mm resulting in 13.79 cm^3. The measured area of the magnetization loop is calibrated by means of a multiplicative factor obtained from the calorimetric measurements. The calibration factor is constant for the entire frequency range. Figure 12 shows the loss-frequency dependence obtained from calorimetry and

Table 3. Hysteresis loss and coupling loss time constant for the whole sample and three sections after cutting.

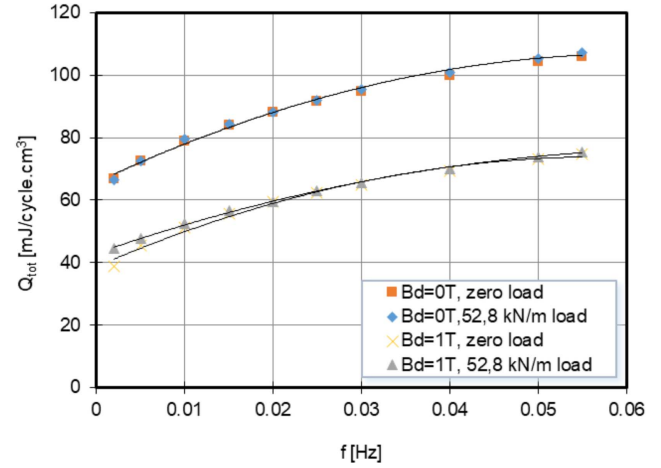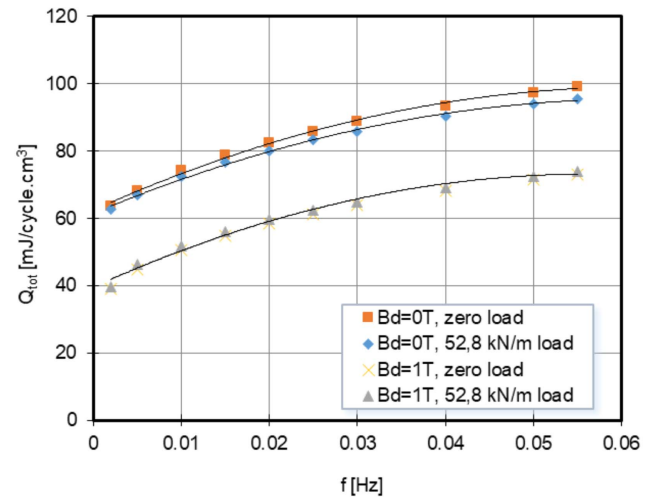|	Whole conductor	End 1	Middle	End 2
Q_h (mJ/cycle · cm^3) $B_d = 0$ T	63	65	63	67
Q_h (mJ/cycle · cm^3) $B_d = 1$ T	39	39	39	41
Coupling loss time constant $n\tau$ (ms) $B_d = 0$ T	550	370	470	430
Coupling loss time constant $n\tau$ (ms) $B_d = 1$ T	460	470	470	490
Calculated sample volume (cm^3)	13.79	4.68	4.62	4.49
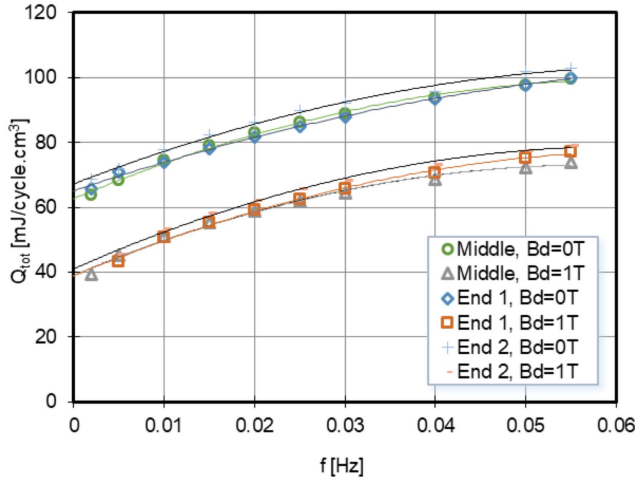
Figure 13. Total AC loss as a function of applied magnetic field frequency for the three conductor sections after cutting.

Figure 15. Comparison of the AC loss between the sample before loading and with an applied load of 53 kN m^{-1}. The magnetic field orientation is parallel to the applied load.

Figure 14. AC loss comparison between whole conductor and average loss value over the three conductor sections after cutting.

Figure 16. Comparison of the AC loss between the sample before loading and with an applied load of 53 kN m^{-1}. The magnetic field orientation is perpendicular to the applied load.

magnetization. Both methods are in good agreement. The lines through the data points at figure 12 are second order polynomial fits of the magnetization data. From the initial slope at low frequency, we obtain the coupling loss time constant $n\tau$ [30] from the sinusoidal magnetic field cycle of amplitude B_a:

$$n\tau = \alpha \frac{\mu_0}{2\pi^2 B_a^2} \qquad (3)$$

where α is the initial slope of the loss-frequency line.

The hysteresis loss and $n\tau$ values for the whole conductor section are presented in table 3.

To check the conductor uniformity, the sample was cut into three segments with practically similar length, referred to as End 1, Middle and End 2. Figure 12 shows the total AC loss of the conductor sections as a function of the applied magnetic field frequency with only the magnetization data shown for clarity. The conductor sections have similar behavior, which indicates good uniformity of the initial whole conductor length (see figure 13). The loss-frequency data was fit by second order polynomials to determine the hysteresis
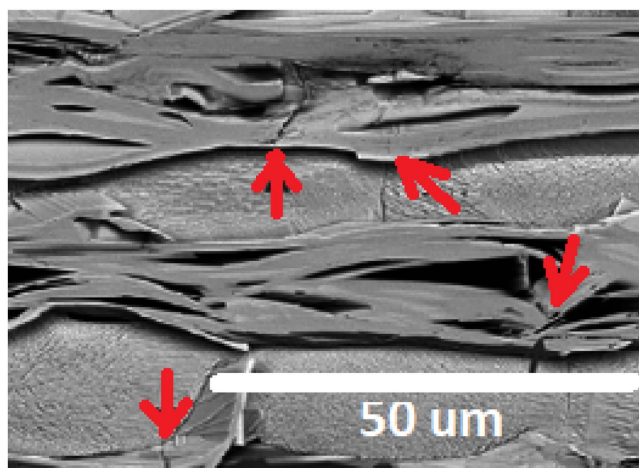
Figure 17. SEM cross-sectional micrograph of most deformed Bi2212 strand segment extracted from the mechanically loaded conductor: cracks on Bi2212 filaments are indicated with red arrows.

loss and coupling loss time constant for each conductor section individually. Table 3 summarizes the hysteresis loss and coupling loss time constant values for the whole conductor and after separating it into three sections.

Figure 14 shows the AC loss comparison between the whole conductor and the average value of the three conductor sections, showing good agreement.

4.3. AC loss measurements under transverse load

The AC loss of the center section was measured under transverse load in order to simulate the effect of the Lorentz force on the conductor. A force of 6.6 kN was applied to the 125 mm sample length resulting in 53 kN m^{-1}. The AC loss under applied load was measured for two orientations of magnetic field to force. The first configuration is performed with magnetic field oriented parallel with the applied load; the second configuration is with the magnetic field perpendicular directed to the applied load. The results of the first configuration are shown in figure 15, while figure 16 shows the data of the second configuration. No significant influence of the applied load on the AC loss of the Bi2212 conductor was observed compared to the non-loaded condition. Considering the 53 kN m^{-1} force and contact area between the transverse load setup and conductor jacket, the peak stress on the conductor is 30–40 MPa, which is around twice the stress on the ITER CSMC conductor under EM load [31]. Several Bi2212 strand segments with severe deformation were extracted from the loaded conductor for preparation of cross-sectional micrographs by scanning electron microscopy (SEM). Clear evidence of cracks on Bi2212 filaments have been found (see figure 17). Similar behavior for transverse load on hysteresis loss was also found for ITER TF CICC showing no effect of cracks in filaments on the hysteresis loss [32]. However, for coupling loss, there are clear effects observed at cycled EM or mechanical loads for ITER CICCs already after the first load during cycling [33]. Meanwhile, there is no evident observable effect on the coupling loss for this Bi2212 conductor at applied

transverse mechanical load (not cycled). This is likely due to the nature of the contact surface of strands, which is obviously different form the Cr-plated Nb$_3$Sn wires in ITER CICCs and requires further investigation. For the conductor, there is no coating or insulating material on the wire. After heat treatment, the wires are stuck together. This could lead to limited movement of strands under transverse load, thus result in no significant change on contact area and resistance among strands. Furthermore, the intra-strand (i.e. inter-filament) coupling loss will be investigated for Bi2212 wire with the cable length ∼418 mm, to identify which is the dominant coupling loss for Bi2212 cable, intra-strand or inter-strand coupling loss. It was not possible to be conclusive on the possible change of transport properties under applied load from these tests, since the Bi2212 conductor was cut to three pieces which were too short for an I_c test. Further investigations are also considered to see the impact of transverse load on transport properties (I_c, T_{cs}) of Bi2212 conductors.

5. Conclusions

One sub-size Bi2212 conductor has been manufactured with 42 twisted Bi2212 wires in three cable stages. The critical current reached 13.1 kA at 4.2 K and self-field, with around 15% critical current degradation by cabling and compaction compared to the evaluated critical current of 15.4 kA based on witness wire performance. The AC loss of Bi2212 wire was measured by VSM at various temperatures. Then, the AC loss of the Bi2212 conductor was measured on the whole conductor length first and then on three conductor sections with similar length individually after cutting. The AC loss comparison between the three conductor sections shows similar behavior, which confirms good sample uniformity along the length. The AC loss under applied load was measured for one conductor section and no significant effect of transverse load up to 53 kN m^{-1} on the conductor AC loss was observed. Both the hysteresis loss and coupling loss remain unchanged. These first AC loss results provide essential properties for the development of Bi2212 CICC and its application in fusion magnets. Further investigations on conductor manufacture will be conducted to achieve better conductor performance.

ORCID iDs

Jinggang Qin ● https://orcid.org/0000-0002-5652-3447

References

[1] Wan Y 2012 Mission of CFETR *ITER Training Forum & Second Workshop on MFE Development Strategy (Hefei, September 6)*

[2] Wu S and Song Y 2012 Concept design of CFETR tokamak machine *ITER Training Forum & Second Workshop on MFE Development Strategy (Hefei, September 6)*

[3] Li J *et al* 2015 Chinese program on CFETR *SOFE2015 (Austin TX, USA, May 31–June 4)*

[4] Miao H, Huang Y, Hong S and Parrell J A 2013 Recent advances in Bi-2212 round wire performance for high field application *IEEE Trans. Appl. Supercond.* **23** 6400104

[5] Hasegawa T, Koizumi T, Hikichi Y, Nakatsu T, Scanlan R, Hirano N and Nagaya S 2002 HTS conductors for magnets *IEEE Trans. Appl. Supercond.* **12** 1136

[6] Ray J-M *et al* 2009 Critical current measurement in HTS Bi2212 ribbons and round wires *IEEE Trans. Appl. Supercond.* **19** 3088–93

[7] Lu X F *et al* 2011 Electromechanical characterization of Bi-2212 strands *IEEE Trans. Appl. Supercond.* vol 21 (no. 3)

[8] Devred A *et al* 2014 Challenges and status of ITER conductor production *Supercond. Sci. Technol.* **27** 044001

[9] Wu Y *et al* 2016 Status of the ITER conductors in China *IEEE Trans. Appl. Supercond.* **26** 6000405

[10] Isono T *et al* 2003 Development of 10 kA Bi2212 conductor for fusion application *IEEE Trans. Appl. Supercond.* **13** 1512–5

[11] Kim S-C *et al* 2009 Fabrication and properties of Bi2212 Rutherford superconducting cable *IEEE Trans. Appl. Supercond.* **19** 3076–9

[12] Barzi E, Lombardo V, Turrioni D, Baca F J and Holesinger T G 2011 BSCCO-2212 wire and cable studies *IEEE Trans. Appl. Supercond.* **21** 2335–9

[13] Kim S-C, Ha D-W, Oh S-S, Song K-J, Kim S-J, Han I-Y and Sohn H-S 2009 Fabrication and properties of Bi2212 Rutherford superconducting cable *IEEE Trans. Appl. Supercond.* **19** 3076–9

[14] Shen T *et al* 2015 High strength kiloampere $Bi_2Sr_2CaCu_2O_x$ cables for high-field magnet applications *Supercond. Sci. Technol.* **28** 065002

[15] Sugano M *et al* 2006 Irreversible behavior of thermal expansion in Bi2212 composite wire at low temperature *Physica* C **445–8** 751–5

[16] wesche R, Fuchs A M, Jakob B and Pasztor G 1996 Axial and bending strain effects in Ag and AgNiMgl Bi-2212 wires *Cryogenics* **36** 419–26

[17] Shen T *et al* 2010 Filament to filament bridging and its influence on developing high critical current density in multifilamentary Bi2Sr2CaCu2O8+x round wires *Supercond. Sci. Technol.* **23** 025009

[18] Liu P *et al* 2017 Research on the mechanical properties of jacket used for Bi2212 cable-in-conduit conductor *IEEE Trans. Appl. Supercond.* **27** 7800204

[19] Qin J *et al* 2017 Manufacture and test of Bi-2212 cable-in-conduit conductor *IEEE Trans. Appl. Supercond.* **27** 4801205

[20] 2004 Vibrating Sample Magnetometer (VSM) Option User's Manual https://web.njit.edu/~tyson/PPMS_Documents/PPMS_Manual/1096-100%20Rev.%20A3%20VSM.pdf

[21] Zieba A and Foner S 1982 Detection coil, sensitivity function, and sample geometry effects for vibrating sample magnetometers *Rev. Sci. Instrum.* **53** 1344

[22] Campbell A M 1995 AC lossese in high Tc superconductors *IEEE Trans. Appl. Supercond.* **5** 682–7

[23] Ries G 1977 AC-losses in multifilamentary superconductors at technical prequencies *IEEE Trans. Magn.* **13** 524–6

[24] Wessel S, Nijhuis A, Ilyin Y, Abbas W, ten Haken B and ten Kate H H J 2004 A novel 'test arrangement for strain influence on strands' (TARSIS): mechanical and electrical testing of ITER Nb_3Sn strands *Adv. Cryog. Eng., Mater.* **50** 466–73

[25] Nijhuis A, Ilyin Y and Wessel W A J 2006 Spatial periodic contact stress and critical current of a Nb_3Sn strand measured in TARSIS *Supercond. Sci. Technol.* **19** 1089–96

[26] van den Eijnden N, Nijhuis A, Ilyin Y, Wessel W A J and ten Kate H H J 2005 Axial tensile stress strain characterization of ITER model coil type Nb_3Sn strands in TARSIS *Supercond. Sci. Technol.* **18** 1523–32

[27] Nijhuis A, Ilyin Y, Wessel W A J and Abbas W 2006 Critical current and strand stiffness of three types Nb_3Sn strand subjected to spatial periodic bending *Supercond. Sci. Technol.* **19** 1136–45

[28] Godeke A, Dhalle M, Morelli A, Stobbelaar L, van Weeren H, van Eck H J N, Abbas W, Nijhuis A, den Ouden A and ten Haken B 2004 A device to investigate the axial strain dependence of the critical current density in superconductors *Rev. Sci. Instrum.* **75** 5112–8

[29] Nijhuis A, Wessel W A J, Ilyin Y, den Ouden A and ten Kate H H J 2006 Critical current measurement with spatial periodic bending imposed by electromagnetic force on a standard test barrel with slots *Rev. Sci. Instrum.* **77** 054701

[30] Verweij A P 1995 Electrodynamics of superconducting cables in accelerator magnets *PhD Thesis* University of Twente

[31] Nijhuis A *et al* 1999 Electromagnetic and mechanical characterisation of ITER CS-MC conductors affected by transverse cyclic loading, part 3: mechanical properties *IEEE Trans. Appl. Supercond.* **9** 165–8

[32] Zhou C, Bink D, Liu B, Miyoshi Y, Wessel W A J, Krooshoop H J G and Nijhuis A 2012 Magnetization measurements on ITER Nb_3Sn CICC and strands subjected to irreversible strain degradation *Supercond. Sci. Technol.* **25** 075004

[33] Yagotintsev K A *et al* AC loss verification tests of ITER CICC superconductors with transverse loading up to 30 000 cycles *Supercond. Sci. Technol.* **30** 115012